LBM – Discrete Dynamics and Finite Difference Method

Michael Junk*

Abstract

With the lattice Boltzmann method, approximate solutions to the incompressible Navier-Stokes equation can be obtained based on discrete microscopic models of gases. The aim of this article is to analyze the LBM approach and show that it is closely related to standard methods like explicit finite difference discretizations and relaxation systems. The new insight into the method allows to extract elements of LBM and to use them in standard schemes like Chorin's projection method.

1 Introduction

In recent years, the lattice Boltzmann method (LBM) has been proposed as potential alternative to conventional solvers for hydrodynamic problems [1, 2, 7]. The basic idea of the method is the numerical simulation of a very simple, fully discrete, microscopic gas model which is nevertheless capable of correctly describing macroscopic flow behavior.

However, if LBM is considered mainly as a numerical method to solve equations of fluid dynamics, like the Navier-Stokes equation, it is natural to ask for its relation to already existing schemes. Based on the frequently used D2Q9 model (nine discrete velocities in two space dimensions), the close relation between LBM and standard methods is demonstrated. It turns out that the discrete modeling in the derivation of the lattice Boltzmann method leads to an explicit finite difference discretization of the Navier-Stokes equation which operates in the stability constellation $\Delta t = \mathcal{O}(\Delta x^2)$. The stencils which appear in the discretization have an interesting structure and they always involve diagonal neighbors. Since conservation properties

*FB Mathematik, Universität Kaiserslautern, Erwin-Schrödingerstraße, 67663 Kaiserslautern, Germany,(junk@mathematik.uni-kl.de).

are taken care of in the modeling step, the resulting scheme shares these properties. Adopting lattice Boltzmann stencils in other schemes is possible and can have positive effects as demonstrated for Chorin's projection method.

2 The Lattice Boltzmann Algorithm

We concentrate on two-dimensional flows for notational simplicity. The first discrete aspect of the lattice Boltzmann model concerns the material itself which is assumed to consist of microscopic particles. These particles can only stay at discrete nodes of a regular lattice (see Fig. 1).

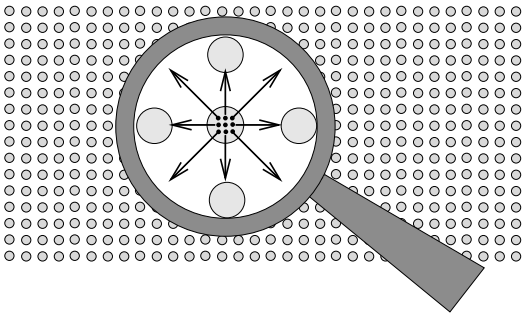

Figure 1: Regular lattice and discrete velocities

In each discrete time step, the particles can move to a neighboring site or stay at their node which gives rise to nine possible velocities $\boldsymbol{C}_0, \ldots, \boldsymbol{C}_8 \in \{-1, 0, 1\}^2$. Consequently, the state of the particle system at time $t \in \mathbb{N}$ is characterized by the densities N_i of particles with velocity $\boldsymbol{C}_i$ at each node $\boldsymbol{x}$ of the grid (see Fig. 2).

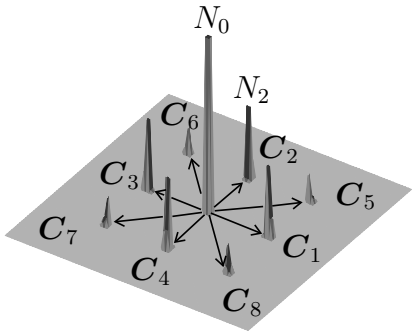

Figure 2: Discrete mass distribution

Macroscopic quantities like the total mass density ρ or the average velocity $\boldsymbol{u}$ are then given as averages of the microscopic densities

$$\rho = \sum_{i=0}^{8} N_i, \qquad \boldsymbol{u} = \sum_{i=0}^{8} N_i \boldsymbol{C}_i / \rho.$$

The state evolution consists of two steps: in the collision phase, atoms arising from neighboring nodes interact instantaneously and may change their velocities which leads to a local redistribution of the densities N_i (Fig. 3).

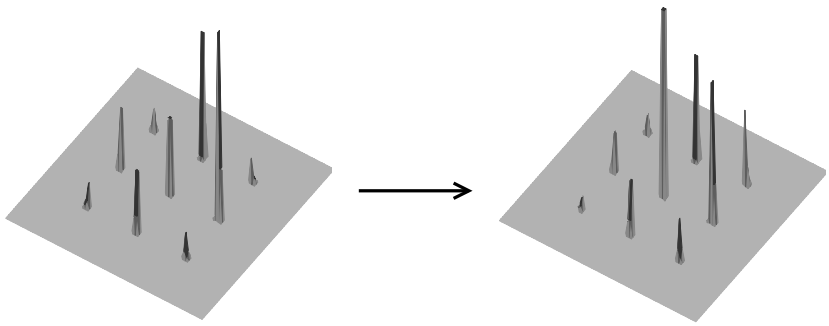

Figure 3: Redistribution of atoms during a collision

During this collision process, total mass and momentum are unchanged. The tendency in this interaction is towards an equilibrium distribution

$$N_i^{eq} = N_i^* \left(\rho + 3\rho \boldsymbol{u} \cdot \boldsymbol{C}_i + \frac{9}{2} \rho \boldsymbol{u} \otimes \boldsymbol{u} : (\boldsymbol{C}_i \otimes \boldsymbol{C}_i - I/3) \right) \tag{1}$$

and is modeled by a simple relaxation. In (1), the quantities N_i^* are constants (4/9 for the zero velocity, 1/9 for the velocities of length one, and 1/36 for those of length $\sqrt{2}$), I is the identity matrix, $\boldsymbol{u} \otimes \boldsymbol{u}$ is a matrix with entries $u_i u_j$ and $A : B = \sum_{i,j} A_{ij} B_{ij}$ denotes the matrix scalar product. We remark that equilibrium distributions for other lattices practically have the same structure and differ only in the constants so that the following considerations carry over to other models.

After collision, the atoms move in a discrete time step to neighboring sites. The combination of the two steps leads to the evolution

$$N_i(t+1, \boldsymbol{x} + \boldsymbol{C}_i) = N_i(t, \boldsymbol{x}) + \omega (N_i^{eq}(t, \boldsymbol{x}) - N_i(t, \boldsymbol{x})) \tag{2}$$

The simplest method to incorporate solid wall boundary conditions is the *bounce back* step: atoms which move towards the boundary are simply reflected to their original node.

If the average velocity $\boldsymbol{u}$ in this process is small compared to the microscopic velocities, one obtains an approximate Navier-Stokes solution where the variations in the density are related to the pressure and the viscosity is controlled by ω. Usually, this behavior is explained by performing a Chapman-Enskog expansion of (2) under the assumption of small Knudsen and Mach number (see [7]). However, it is also possible to relate the algorithm (2) directly to a discretization of the Navier-Stokes equation. This approach is presented in the following section.

3 Consistency Analysis of LBM

In order to recover a discretization of the Navier-Stokes equation from (2), two main steps are necessary: a change of scales and a change of variables. In the lattice Boltzmann evolution (2), time and space scales are chosen in view of the microscopic movement of the particles. In particular, the time step is $\Delta t_{LB} = 1$ and since $\boldsymbol{C}_i \in \{-1, 0, 1\}^2$, the distance between nodes is $\Delta x_{LB} = 1$ (to obtain a fine discretization, a typical length L of the underlying problem therefore satisfies $L \gg 1$). The small Mach number assumption implies that a typical average speed U is small compared to the sound speed which is related to the speed of the particles (we introduce $\epsilon = U$ as small parameter). While these scales are very reasonable for the implementation of the method, they are not related to the underlying Navier-Stokes problem. If we consider for example the flow around a circular disk (see Fig. 4),

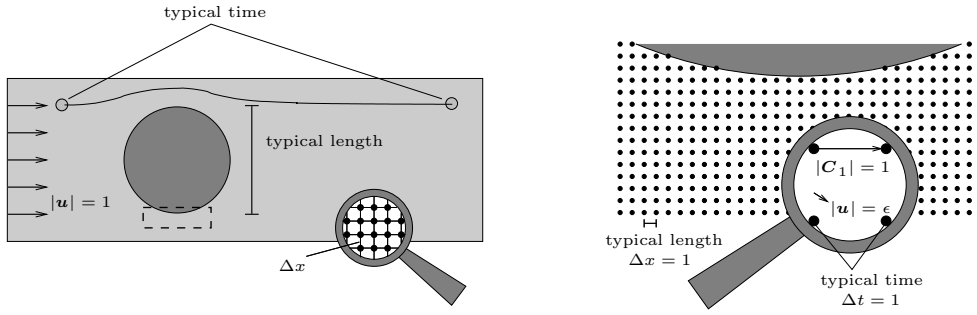

Figure 4: Navier-Stokes and Lattice Boltzmann scales

a typical length L is given by the diameter of the disk, a typical speed U is the inflow velocity, and the related typical time scale T is given by the time required to travel a distance of several L with speed U. Assuming that L and U are given in lattice Boltzmann scales, we find the Navier-Stokes

space and time steps

$$\Delta x = \frac{\Delta x_{LB}}{L} = \frac{1}{L}, \qquad \Delta t = \frac{\Delta t_{LB}}{T} = U\frac{\Delta t_{LB}}{L} = U\frac{1}{L} = U\Delta x.$$

In [6] it was shown that $\epsilon = \mathcal{O}(\Delta x)$ is necessary in order to get consistency of LBM with the Navier-Stokes equation. We thus conclude that in the problem related scales the stability condition $\Delta t = \mathcal{O}(\Delta x^2)$ known from explicit discretizations of parabolic equations is recovered. Changing the scales in (2), we end up with the evolution

$$N_i(t + \Delta t, \boldsymbol{x} + \Delta x\, \boldsymbol{C}_i) = [N_i + \omega(N_i^{eq}(\rho, \epsilon\boldsymbol{u}) - N_i)]_{(t,\boldsymbol{x})} \tag{3}$$

In the second step, we change the lattice Boltzmann variables N_i in (3) to problem related variables. Of primary interest is, of course, the velocity field $\boldsymbol{u}$ and the pressure p, or equivalently, the momentum $\boldsymbol{m} = \rho\boldsymbol{u} = \sum_i N_i\boldsymbol{C}_i$ and the density $\rho = \sum_i N_i$ which is proportional to p in lattice Boltzmann models. Note that both ρ and $\boldsymbol{m}$ depend linearly on the densities N_i. In order to obtain a set of variables which includes the quantities ρ and $\boldsymbol{m}$ and which is equivalent to $\boldsymbol{N} = (N_0, \ldots, N_8)$, we consider additional linear functionals of the distribution $\boldsymbol{N}$. For example, we introduce the symmetric tensor

$$\theta = \sum_i N_i(\boldsymbol{C}_i \otimes \boldsymbol{C}_i - I/3)$$

which yields three independent linear functionals. In a similar manner, we can define two third order and one fourth order moment giving rise to three more variables $\boldsymbol{w}$ (for details see [4]). Altogether, a linear invertible mapping $\boldsymbol{N} \mapsto (\rho, \boldsymbol{m}, \theta, \boldsymbol{w})$ is obtained. Applying the variable transformation to the evolution (3), the finite difference expressions in N_i turn into finite difference expressions in the new variables.

In order to illustrate this transformation process, let us consider a very much simplified version of (3) where we set $\omega = 1$ and $N_i^{eq} = N_i^*\rho$

$$N_i(t + \Delta t, \boldsymbol{x} + \Delta x\, \boldsymbol{C}_i) = N_i^*\rho(t, \boldsymbol{x}). \tag{4}$$

The corresponding evolution of the density $\rho = \sum_i N_i$ has the form

$$\rho(t + \Delta t, \boldsymbol{x}) = \sum_i N_i(t + \Delta t, \boldsymbol{x}) = \sum_i N_i^*\rho(t, \boldsymbol{x} - \Delta x\, \boldsymbol{C}_i)$$

Note that the last expression involves the evaluation of ρ at all neighboring nodes of $\boldsymbol{x}$ with certain weights N_i^*. This is a standard finite difference

expression which can also be written using a finite difference stencil. With the definition of the N_i^*, we get

$$\rho(t+\Delta t,\boldsymbol{x}) = \rho(t,\boldsymbol{x}) + \frac{1}{36}\begin{bmatrix}1 & 4 & 1\\ 4 & -20 & 4\\ 1 & 4 & 1\end{bmatrix}\rho(t,\boldsymbol{x}).$$

Subtracting $\rho(t,\boldsymbol{x})$ on both sides and dividing by Δt, we find

$$\frac{\rho(t+\Delta t,\boldsymbol{x})-\rho(t,\boldsymbol{x})}{\Delta t} = \frac{1}{6}\frac{\Delta x^2}{\Delta t}\tilde{\Delta}\rho(t,\boldsymbol{x})$$

where $\tilde{\Delta}$ is the standard nine-point stencil of the Laplacian. Consequently, if N_i follows the evolution (4), the total density is the solution of a finite difference discretization of the diffusion equation $\partial_t\rho = \nu\Delta\rho$ if $\Delta t = 6\Delta x^2/\nu$. Applying the same analysis to the more complicated evolution (3), we find that the moments ρ and $\boldsymbol{m} = \rho\boldsymbol{u}$ evolve, up to terms of order $\mathcal{O}(\epsilon^2)$, according to the equations

$$\frac{\partial\rho}{\partial t} + \operatorname{div}\rho\boldsymbol{u} = \frac{1}{6}\Delta\rho$$
$$\frac{\partial\rho\boldsymbol{u}}{\partial t} + \operatorname{div}\left(\omega\rho\boldsymbol{u}\otimes\boldsymbol{u} + (1-\omega)\theta\right) + \frac{\nabla\rho}{3\epsilon^2} = \frac{1}{6}(\Delta + 2\nabla\operatorname{div})\rho\boldsymbol{u} - \frac{\nabla\Delta\rho}{18}$$

The higher moments satisfy similar equations with hyperbolic operators on the left hand side but since they are not conservative quantities, source terms of relaxation type appear on the right hand side. For example, the equation for θ has the structure

$$\frac{\partial\theta}{\partial t} + \operatorname{div}\Pi = -\frac{\omega}{\epsilon^2}\left(\theta - \rho\boldsymbol{u}\otimes\boldsymbol{u} + \frac{2}{3\omega}S[\rho\boldsymbol{u}]\right) - \frac{1}{27\epsilon^2}\nabla\otimes\nabla\rho + \mathcal{O}(1)$$

where $S_{ij} = (\partial_{x_j}\rho u_i + \partial_{x_i}\rho u_j)/2$, Π depends on the additional variables $\boldsymbol{w}$, and the term $\mathcal{O}(1)$ involves derivatives of $\rho\boldsymbol{u}, \theta$ and $\rho\boldsymbol{u}\otimes\boldsymbol{u}$. Analyzing the equations for small ϵ, we find that $\theta = \rho\boldsymbol{u}\otimes\boldsymbol{u} - \frac{2}{3\omega}S[\rho\boldsymbol{u}] + \mathcal{O}(\epsilon^2)$ and that $\nabla\rho = \mathcal{O}(\epsilon^2)$. The latter condition can be reformulated by introducing the pressure p through $\rho = \bar{\rho}(1+3\epsilon^2 p)$ where $\bar{\rho}$ is some constant. Using these relations, the moment equations transform into

$$\operatorname{div}\boldsymbol{u} = \mathcal{O}(\epsilon^2), \quad \frac{\partial\boldsymbol{u}}{\partial t} + \operatorname{div}\boldsymbol{u}\otimes\boldsymbol{u} + \nabla p = \frac{1}{3}\left(\frac{1}{\omega}-\frac{1}{2}\right)\Delta\boldsymbol{u} + \mathcal{O}(\epsilon^2) \qquad (5)$$

which are the Navier-Stokes equations in leading order. In analogy to the simple diffusion example, the transformation of variables in (3) also shows

how the differential operators in (5) are approximated by finite difference stencils. The discrete version of (5) turns out to be

$$\frac{1}{12\Delta x}\left(\begin{bmatrix}-1&0&1\\-4&0&4\\-1&0&1\end{bmatrix}u_1^n+\begin{bmatrix}1&4&1\\0&0&0\\-1&-4&-1\end{bmatrix}u_2^n\right)=\mathcal{O}(\epsilon^2)$$

$$\frac{u_1^{n+1}-u_1^n}{\Delta t}+\frac{1}{12\Delta x}\begin{bmatrix}-1&0&1\\-4&0&4\\-1&0&1\end{bmatrix}u_1^nu_1^n+\frac{1}{4\Delta x}\begin{bmatrix}1&0&1\\0&0&0\\-1&0&-1\end{bmatrix}u_1^nu_2^n+\frac{1}{36\Delta x}\begin{bmatrix}-1&0&1\\-4&0&4\\-1&0&1\end{bmatrix}p^n$$

$$=\left(\frac{1}{36\Delta x^2}\begin{bmatrix}1&4&1\\4&-20&4\\1&4&1\end{bmatrix}+\frac{1/\omega-1}{216\,\Delta x^2}\begin{bmatrix}5&0&8&0&5\\4&0&-8&0&4\\0&0&-36&0&0\\4&0&-8&0&4\\5&0&8&0&5\end{bmatrix}\right)u_1^n+\mathcal{O}(\epsilon^2)$$

with a similar relation for the second component u_2. Note that both stencils in the discretization of $\operatorname{div}\boldsymbol{u}$ can be viewed as convex combinations of standard central difference approximations. and that the expression $\partial_{x_2}u_1u_2$ is discretized with a different stencil for ∂_{x_2} (the same holds for $\partial_{x_1}u_1u_2$ in the u_2 equation). As a common feature, all stencils involve diagonal neighbors which is due to the underlying set of discrete velocities. Finally, the viscous Laplacian consists of a fixed contribution based on the nine-point Laplacian and a 25-point stencil which has its origin in the expression $\operatorname{div}S[\boldsymbol{u}]$ and which can be controlled by the collision parameter ω (the unusual size is due to the combination of the discrete divergence and discrete derivatives in the components of S). For $\omega>1$, it has an anti-diffusive influence to counteract the nine-point Laplacian.

An interesting result follows from the observation that lattice Boltzmann solutions do not exhibit any pressure oscillations which are known to appear in schemes for the Navier-Stokes equation which use non-staggered grids to store velocity and pressure variables. One might suspect that this is due to the unusual form of the stencils. In the following section, this hypothesis is supported by using the lattice Boltzmann stencils in connection with Chorin's projection method for the Stokes equation.

4 Extracting Lattice Boltzmann Ideas

A standard approach to solve the Stokes (or Navier-Stokes) equation numerically is Chorin's projection method [3]. In this approach, the temporal discretization is semi-implicit

$$\boldsymbol{u}^{n+1}(\boldsymbol{x})=\boldsymbol{u}^n(\boldsymbol{x})-\nabla p^{n+1}(\boldsymbol{x})+\nu\Delta\boldsymbol{u}^n(\boldsymbol{x}). \tag{6}$$

The pressure is determined from $\operatorname{div}\boldsymbol{u}^{n+1}=\operatorname{div}\boldsymbol{u}^n=0$ and (6)

$$\operatorname{div}\nabla p^{n+1}=\nu\operatorname{div}\Delta\boldsymbol{u}^n. \tag{7}$$

Discretizing Δ in (6) with the five-point Laplacian and the first derivatives with standard central differences

$$\frac{\partial}{\partial x_1} \approx \frac{1}{2\Delta x} \begin{bmatrix} -1 & 0 & 1 \end{bmatrix}, \qquad \frac{\partial}{\partial x_2} \approx \frac{1}{2\Delta x} \begin{bmatrix} 1 \\ 0 \\ -1 \end{bmatrix}$$

one is naturally led to a wide Laplacian in equation (7)

$$\Delta \approx \frac{1}{\Delta x^2} \begin{bmatrix} & & 1 & & \\ & & 0 & & \\ 1 & 0 & -4 & 0 & 1 \\ & & 0 & & \\ & & 1 & & \end{bmatrix},$$

by iterating discrete divergence and discrete gradient. If half-sided stencils are used near the boundary of the domain, it is well known that the resulting numerical solution exhibits pressure oscillations which reduce the accuracy to first order in pressure (for details see [8]). The reason is that the wide Laplacian essentially splits the grid into two independent sub-grids, on each of which the pressure Poisson equation is solved with boundary conditions which differ in third order. These slight differences are then amplified by the viscous five point Laplacian and reappear in first order.

To give an example, we consider the test problem presented in [8] where (6) is solved in $\Omega = (0,1) \times (0,1)$ with no-slip conditions $\boldsymbol{u} = 0$ on the top and bottom boundaries and periodic conditions in horizontal direction. As initial conditions, we choose

$$\begin{aligned} u_1(x_1, x_2) &= 6x_2(1 - x_2) + 16(2x_2 - 6x_2^2 + 4x_2^3)\sin(2\pi x_1)/2\pi, \\ u_2(x_1, x_2) &= -16(x_2^2 - 2x_2^3 + x_2^4)\cos(2\pi x_1). \end{aligned}$$

Taking a MAC-solution with a fine discretization as exact solution, we calculate the error with the standard discretization of Chorin's method at time $t = 1$ on a 32×32 grid (see Fig. 5). Clearly, the error is strongly oscillating. If, on the other hand, we use the lattice Boltzmann stencils

$$\frac{\partial}{\partial x_1} \approx \frac{1}{12\Delta x} \begin{bmatrix} -1 & 0 & 1 \\ -4 & 0 & 4 \\ -1 & 0 & 1 \end{bmatrix}, \qquad \frac{\partial}{\partial x_2} \approx \frac{1}{12\Delta x} \begin{bmatrix} 1 & 4 & 1 \\ 0 & 0 & 0 \\ -1 & -4 & -1 \end{bmatrix},$$

for divergence and gradient and the 25-point Laplacians to discretize

$$\Delta u_1 \approx \frac{1}{72\Delta x^2} \begin{bmatrix} 5 & 0 & 8 & 0 & 5 \\ 4 & 0 & -8 & 0 & 4 \\ 0 & 0 & -36 & 0 & 0 \\ 4 & 0 & -8 & 0 & 4 \\ 5 & 0 & 8 & 0 & 5 \end{bmatrix} u_1, \qquad \Delta u_2 \approx \frac{1}{72\Delta x^2} \begin{bmatrix} 5 & 4 & 0 & 4 & 5 \\ 0 & 0 & 0 & 0 & 0 \\ 8 & -8 & -36 & -8 & 8 \\ 0 & 0 & 0 & 0 & 0 \\ 5 & 4 & 0 & 4 & 5 \end{bmatrix} u_2,$$

then the oscillating errors induced by the Laplacian in (7) which is obtained by combining discrete divergence and gradient

$$\Delta \approx \frac{1}{72\Delta x^2} \begin{bmatrix} 1 & 4 & 8 & 4 & 1 \\ 4 & 0 & -8 & 0 & 4 \\ 8 & -8 & -36 & -8 & 8 \\ 4 & 0 & -8 & 0 & 4 \\ 1 & 4 & 8 & 4 & 1 \end{bmatrix}$$

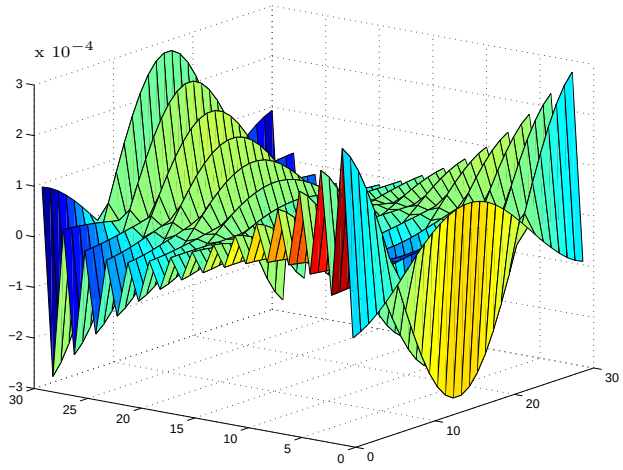

Figure 5: Error using the standard discretization

is no longer amplified. The corresponding error in the pressure is shown in Fig. 6. For a detailed alternating error analysis and a numerical convergence study, we refer to [5].

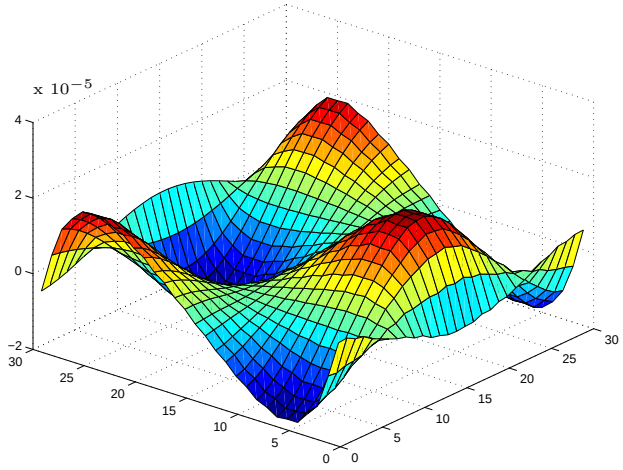

Figure 6: Error using lattice Boltzmann stencils

References

[1] R. Benzi, S. Succi, and M. Vergassola. The Lattice-Boltzmann equation: Theory and applications. *Physics Reports*, 222:145–197, 1992.

[2] S. Chen and G.D. Doolen. Lattice Boltzmann method for fluid flows. *Ann. Rev. Fluid Mech.*, 30:329–364, 1998.

[3] A.J. Chorin. Numerical solution of the Navier-Stokes equations. *Math. Comp.*, 22:745–762, 1968.

[4] M. Junk. A finite difference interpretation of the lattice Boltzmann method. *Numer. Methods Partial Differ. Equations*, to appear.

[5] M. Junk and A. Klar. Discretization for the incompressible navier-stokes equations based on the lattice boltzmann method. *SIAM J. Sci. Comp.*, to appear.

[6] M. Reider and J. Sterling. Accuracy of discrete velocity BGK models for the simulation of the incompressible Navier Stokes equations. *Computers and Fluids*, 24:459–467, 1995.

[7] D. H. Rothman and S. Zaleski. *Lattice-Gas Cellular Automata*. Cambridge University Press, 1997.

[8] B. Wetton. Analysis of the spatial error for a class of finite difference methods for viscous incompressible flow. *SIAM J. Num. Anal.*, 34:723–755, 1997.